

RESEARCH ARTICLE

10.1002/2016SW001593

Special Section:

Reprise of 2001 Space Weather Monograph

Key Points:

- New models for the F_2 peak height $h_m F_2$ in IRI-2016
- Development of the Real-Time International Reference Ionosphere (IRI)
- Improved description of IRI ion composition at low and high solar activities

Correspondence to:

D. Bilitza,
dbilitza@gnu.edu

Citation:

Bilitza, D., D. Altadill, V. Truhlik, V. Shubin, I. Galkin, B. Reinisch, and X. Huang (2017), International Reference Ionosphere 2016: From ionospheric climate to real-time weather predictions, *Space Weather*, 15, 418–429, doi:10.1002/2016SW001593.

Received 28 DEC 2016

Accepted 8 FEB 2017

Accepted article online 13 FEB 2017

Published online 27 FEB 2017

Corrected 10 APR 2017

This article was corrected on 10 APR 2017. See the end of the full text for details.

International Reference Ionosphere 2016: From ionospheric climate to real-time weather predictions

D. Bilitza^{1,2} , D. Altadill³ , V. Truhlik⁴, V. Shubin⁵, I. Galkin⁶ , B. Reinisch^{6,7} , and X. Huang^{7,8}

¹Department of Physics and Astronomy, George Mason University, Fairfax, Virginia, USA, ²Heliospheric Laboratory, NASA, Goddard Space Flight Center, Greenbelt, Maryland, USA, ³Observatori de l'Ebre, (OE), CSIC -Universitat Ramon Llull, Roquetes, Spain, ⁴Department of upper atmosphere, Institute of Atmospheric Physics CAS, Prague, Czech Republic, ⁵Pushkov Institute of Terrestrial Magnetism, Ionosphere and Radio-Wave Propagation (IZMIRAN), Russian Academy of Science, Moscow, Russia, ⁶Space Science Laboratory, University of Massachusetts Lowell, Lowell, Massachusetts, USA, ⁷Lowell Digisonde International, LLC, Lowell, Massachusetts, USA, ⁸Deceased 15 October 2016

Abstract The paper presents the latest version of the International Reference Ionosphere model (IRI-2016) describing the most important changes and improvements that were included with this version and discussing their impact on the IRI predictions of ionospheric parameters. IRI-2016 includes two new model options for the F_2 peak height $h_m F_2$ and a better representation of topside ion densities at very low and high solar activities. In addition, a number of smaller changes were made concerning the use of solar indices and the speedup of the computer program. We also review the latest developments toward a Real-Time IRI. The goal is to progress from predicting climatology to describing the real-time weather conditions in the ionosphere.

1. Introduction

The International Reference Ionosphere (IRI) is a joint undertaking by the Committee on Space Research (COSPAR) and the International Union of Radio Science (URSI) with the goal of developing and improving an international standard for the parameters in Earth's ionosphere [Bilitza *et al.*, 2014]. This endeavor was originally triggered by the need for an ionosphere model for the satellite/experiment design and satellite data analysis (COSPAR) and for radio propagation studies (URSI) but has meanwhile found a much broader range of users with space weather concerns. In April 2014 IRI became the official ISO standard for the ionosphere; ISO is the International Standardization Organization. As requested by these international unions, IRI was built as an empirical model representing the syntheses of most of the available ground and space measurements of ionospheric characteristics. IRI represents monthly averages of electron and ion densities and temperatures in the altitude range of 50 km–2000 km. It also provides the vertical total electron content (TEC) from the lower boundary (60–80 km) to a user-specified upper boundary. Additional IRI output includes the ion drift near the magnetic equator and the probability for the occurrence of a F_1 layer and of spread F .

The IRI Working Group consists of 60+ ionospheric experts that includes representatives of the different ground and space ionospheric measurement techniques and the different countries worldwide. The ongoing evaluation and improvement of the IRI model is discussed during biannual workshops that focus on a specific aspect of the modeling problem. Each workshop is generally attended by 100–120 participants (see irimodel.org for more details). The most recent workshop was held as a COSPAR Capacity Building Workshop at the King Mongkut's Institute of Technology Ladkrabang in Bangkok, Thailand, 2–13 November 2015 on the special topic of "Improved Accuracy in the Equatorial Region and Progress Towards a Real-time IRI Model." Presentations from these workshops and other IRI-related papers are published in special issues of *Advances in Space Research (ASR)*, the last one on the topic "International Reference Ionosphere and Global Navigation Satellite Systems" in volume 55, number 8. More details about the IRI project can be found on the IRI homepage at irimodel.org including workshop summaries, references and a list of the special ASR issues, the IRI model code, and related links.

This paper briefly summarizes the improvements that are being introduced with the 2016 version of the IRI model. Most importantly, IRI-2016 presents two new models for the F_2 peak electron density height, $h_m F_2$, and improvements of the ion composition at low and high solar activity. In addition, a number of changes

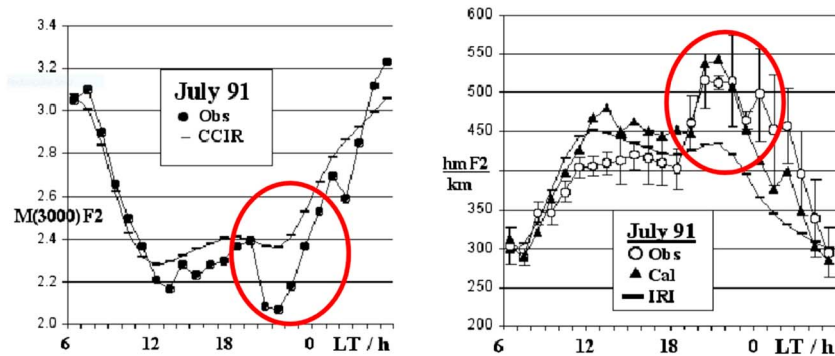


Figure 1. (left) $M(3000)F_2$ ionosonde measurements (dot) and CCIR model predictions (minus) over Ouagadougou, Burkina Faso (latitude: 12.4, longitude: 1.5, dip: 6) in July of 1991; (right) h_mF_2 ionosonde measurements (circle), IRI predictions using CCIR- $M(3000)F_2$ (minus), and using the measured $M(3000)F_2$ (solid triangle) for the same location and time; The red circles highlight the evening drop in $M(3000)F_2$ that is not reproduced in the CCIR model and therefore leads to a significant underestimation of the ionosonde h_mF_2 by IRI.

were made regarding the input and use solar and ionospheric indices, and changes were made to the program code (FORTRAN) to speedup the computation of IRI values. We will also review the progress that is being made toward the development of the Real-Time IRI.

2. New h_mF_2 Models

The height of the F_2 peak, h_mF_2 , is of great importance for many radio propagation studies and applications because it marks the point of highest electron density in the ionosphere. h_mF_2 has also proven to be a valuable source for deriving the neutral wind at middle latitudes [Miller et al., 1986; Richards, 1991; Dyson et al., 1997], and IRI h_mF_2 has been used to produce the global scale meridional wind climatology [Miller et al., 1997]. IRI like most other empirical models has relied on the Consultative Committee on International Radio (CCIR) model [Consultative Committee on International Radio (CCIR), 1967] for the propagation factor $M(3000)F_2$ and on the close correlation between h_mF_2 and $M(3000)F_2$ [Shimazaki, 1955; Bilitza and Eyfrig, 1978; Bilitza et al., 1979; Dudeney, 1983]. $M(3000)F_2$ is defined as $MUF(3000)/f_oF_2$ where $MUF(3000)$ is the highest frequency that, refracted in the ionosphere, can be received at a distance of 3000 km. Like f_oF_2 , $M(3000)F_2$ is routinely scaled from ionograms and therefore a large database exists for this parameter covering several solar cycles. Obtaining h_mF_2 from ionograms requires a more complex analysis involving the scaling and inversion of the ionogram trace. For these reasons CCIR modeling has focused on f_oF_2 and $M(3000)F_2$ rather than h_mF_2 . The CCIR [1967] models for f_oF_2 and $M(3000)F_2$ use the same formalism, and they are based on monthly median values obtained by the worldwide network of ionosondes (about 150 stations) during the years 1954 to 1958. Limitations of this approach for h_mF_2 modeling have been noted in a number of studies [Bilitza, 1985; Adeniyi et al., 2003; Lee and Reinisch, 2006; Brum et al., 2011; Magdaleno et al., 2011; Araujo-Pradere et al., 2013; Ezquer et al., 2014]. Adeniyi et al. [2003] pointed out the three main error sources: (1) the limited data volume available at the time of the model development; (2) the limits in reproducing small scale features in the diurnal variation because of the chosen functional representation (harmonics of up to order 4 only); and (3) the uncertainty introduced with the formula describing the relationship between h_mF_2 and $M(3000)F_2$. Because of error source (2) the current model is not able to reproduce the observed sharp evening peak of h_mF_2 at equatorial latitudes that is related to the reversal in ion drift [Lee and Reinisch, 2006; Abdu et al., 2010]. An example of such a misrepresentation is shown in Figure 1. Regarding error source (3), it is clear that the relationship between h_mF_2 and $M(3000)F_2$ depends on the distribution of ionization below the F_2 peak. Functional descriptions of the relationship have relied on the ratio f_oF_2/f_oE to characterize this distribution. Nevertheless, later work has shown that this is not sufficient and that differences in distribution due to magnetic latitude and solar activity have also to be considered leading to a new model for the relationship [Bilitza et al., 1979] that is used in IRI. However, one has to keep in mind that either one of these models for the h_mF_2 - $M(3000)F_2$ relationship is just an approximation depending on several assumptions [see Dudeney, 1983]. Figure 2 shows an example of a breakdown of the relationship leading to large differences between the observed and IRI model values. Furthermore, during the recent

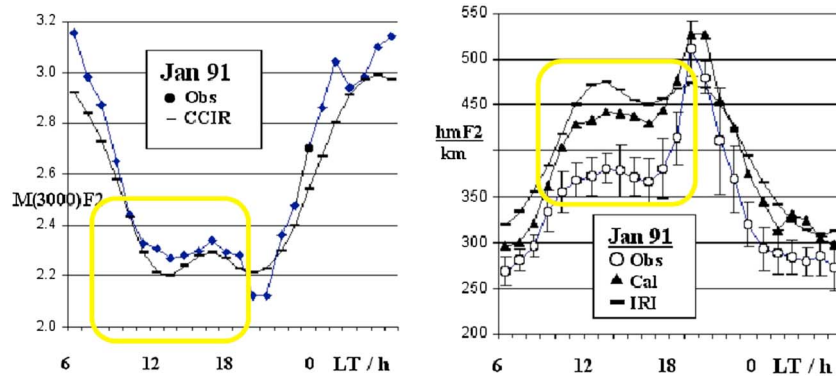


Figure 2. (left) $M(3000)F_2$ ionosonde measurements (dot) and CCIR model predictions (minus) over Ouagadougou, Burkina Faso (latitude: 12.4, longitude: 1.5, dip: 6) in January of 1991; (right) h_mF_2 ionosonde measurements (circle), IRI predictions using CCIR- $M(3000)F_2$ (minus), and using the measured $M(3000)F_2$ (solid triangle) for the same location and time; the yellow squares highlight a time period where the measured $M(3000)F_2$ is well represented by the CCIR model, but the observed h_mF_2 values are significantly overestimated by IRI indicating a breakdown of the relationship between $M(3000)F_2$ and h_mF_2 .

exceptionally low solar minimum in 2008–2009 conditions were reached for which the relationship model used in IRI no longer produced realistic h_mF_2 values. A lower limit of 1.7 was introduced for the ratio f_oF_2/f_oE to keep IRI h_mF_2 values dropping too low. And finally, the use of an $M(3000)F_2$ -based model makes it very difficult to assimilate measured h_mF_2 values, e.g., from incoherent scatter radars, into the IRI model for real-time updating.

Because of these limitations of the IRI h_mF_2 model, the IRI group had given high priority to the development of new h_mF_2 models, and this led to renewed community-wide focus on modeling this important quantity. *Gulyaeva et al.* [2008] developed a model based on topside sounder data from ISIS-1, ISIS-2, IK-19, and Cosmos-1890 from the period 1969–1987 (~90,000 values) describing variations with local time, season, geomagnetic latitude, geodetic longitude, and solar radio flux. Older topside sounder profile data have the shortcoming that they do not reach F_2 peak altitudes and an extrapolation scheme has to be applied to recover the peak density and height. *Gulyaeva et al.* [2008] applied an extrapolation of the first derivative of the topside electron density profile and obtained the layer height where $d\ln[N_e]/d\ln[h]=0$. *Zhang et al.* [2009] applied empirical orthogonal functions for a global representation of the IRI h_mF_2 values. *Hoque and Jakowski* [2012] developed their model based on data from 69 ionosondes and radio occultation data from CHAMP, Gravity Recovery and Climate Experiment (GRACE), and Constellation Observing System for Meteorology, Ionosphere, and Climate (COSMIC). The model uses just 13 coefficients to describe diurnal, annual, semiannual, (magnetic) latitudinal, and solar cycle variations. The models of *Gulyaeva et al.* [2008] and *Hoque and Jakowski* [2012] did well in representing the main variation patterns of h_mF_2 . However, these models are not able to describe the detailed spatial and temporal structure of h_mF_2 variations because of the small number of coefficients used. *Brunini et al.* [2013] took a different approach. They recognized the success and wide use of the CCIR [1967] model for the F_2 peak plasma frequency, f_oF_2 , and applied the same formalism to h_mF_2 values computed with IRI. This turned out to be an important precursor for the real-time h_mF_2 model that will be discussed later in this paper. The CCIR [1967] mapping is based on the pioneering work of *Jones and Gallet* [1962] using a special set of geographic functions in combination with harmonics in UT. A purely ionosonde-based modeling effort was undertaken by *Magdaleno et al.* [2011] and *Altadill et al.* [2013]. Additionally, *Shubin et al.* [2013] presented a h_mF_2 model based on radio occultation data from COSMIC, GRACE, and CHAMP. The last two models have been selected for inclusion in the 2016 version of the IRI model and will be discussed in greater detail in the following sections.

All of these models now represent h_mF_2 directly and no longer depend on the propagation factor $M(3000)F_2$ and its relationship with h_mF_2 , therefore avoiding the error source connected with the $M(3000)F_2$ approach. In addition to these models, which represent the quiet time behavior of h_mF_2 , a number of studies have attempted to describe the changes during storm times including the very promising models of *Blanch and Altadill* [2012] and of *Gulyaeva* [2012] based on digisonde data from the Ebro station in Spain and topside sounder data (from ISIS, IK-19, and COSMOS-1809), respectively.

2.1. The Altadill et al. [2013] h_mF_2 Model (Called AMTB from Hereon)

The AMTB model is based on data from 26 digisonde stations from the Global Ionosphere Radio Observatory (GIRO) network [<http://giro.uml.edu>] [Reinisch and Galkin, 2011] for the time period 1998–2006. In order to obtain monthly averages of quiet time h_mF_2 the Monthly Averaged Representative Profile (MARP) technique [Huang and Reinisch, 1996] was applied. MARP excludes the quarter (25%) of individual $N(h)$ profiles that show the largest deviations from the monthly average and MARP thus removes the profiles most likely related to disturbed ionospheric conditions. The global h_mF_2 variations are represented by spherical harmonics in a reference frame defined by modified dip latitude and longitude. Because the limited number of stations is not sufficient for the spherical harmonics analysis, Altadill et al. [2013] had to fill out the global data coverage with fictitious data points. These data points were established by assuming that differences in local time are equivalent to differences in longitude. So starting from each station, additional data points were added at 15° intervals in longitude (1 h LT) along the station's modified dip latitude. AMTB applies harmonics terms up to order 4 in longitude and 8 in latitude and uses a Fourier expansion of the spherical harmonics coefficients up to order 2 to represent the annual variation. Model coefficients are provided for low and high solar activity (12 month running mean of sunspot number $R_{12} = 15$ and 120), and linear interpolation and extrapolation is suggested for other solar activities. In total the AMTB model consists of 610 coefficients. Compared to the old IRI model, the AMTB model improves the fit to its underlying database by 10% on average and by up to 30% at high and low latitudes. Because of this good performance, AMTB is the recommended h_mF_2 option in IRI-2016.

2.2. The Satellite and Digisonde Model of the F_2 Layer Height (SDMF2)

The SDMF2 model was developed by Shubin et al. [2013] and then extended by Shubin [2015] with a large amount of radio occultation (RO) data from CHAMP (years: 2001–2008; ~300,000 values), GRACE (2007–2011; ~100,000) and COSMIC (2006–2012; ~3,500,000) and with h_mF_2 data from 62 digisondes for the years 1987–2012 from the Digital Ionogram Data Base (<http://ulcar.uml.edu/DIDBase/>). Like other models, SDMF2 describes global variations with spherical harmonics using terms up to order 12 in modified dip latitude and up to order 8 in longitude. A Fourier expansion up to order 3 is used to describe the UT variation of the spherical harmonics coefficients. This is done for each month and for two levels of solar activity ($F_{10.7A} < 80$ and $F_{10.7A} > 120$ where $F_{10.7A}$ is the 81 day average of solar index $F_{10.7}$) leading to a total of 85,824 coefficients. SDMF2 assume a logarithmic dependence on solar activity, which is different from the linear approach of most other models and helps to represent a saturation effect observed at high solar activities. Although the RO technique has made great progress over the last years the use of these data still requires a filtering process to eliminate unrealistic and clearly wrong profiles. Shubin [2015] applies such a process focused on the F_2 peak region of the profiles eliminating 10% of the data. Another problem the SDMF2 developers faced was the uneven distribution in solar activity with the low solar activity subset being much larger than the high one. This was partially compensated by filling out data empty months of the high solar activity subset with seasonal averages. Evaluating his model and IRI with the digisonde data that had not been used for the modeling (from solar activity range $80 < F_{10.7A} < 120$), Shubin [2015] finds an improvement of up to 6% over IRI with the largest improvements in the South African sector. The SDMF2 model is introduced in IRI-2016 as the second new option for h_mF_2 . This will give the IRI user community the ability to compare the different h_mF_2 model predictions against various data sources and eventually help to improve the accuracy of these models and measurement techniques. It also gives an indication how much uncertainty still exists in determining the true h_mF_2 value.

2.3. First Comparisons of the IRI h_mF_2 Model Options

With the inclusion of two new model options for h_mF_2 the first questions are to what extent do these new models overcome the problems of the older $M(3000)F_2$ -based model and how much do these models differ between each other. Figures 3a and 3b show the diurnal variation of the three options for a midlatitude example for summer and winter of a high solar activity year. All three models agree with each other fairly well with the largest differences (20–30 km) at nighttime. During winter the SMDF2 model (called Shubin-2015 in Figures 3–5) is 20–40 km lower than the other two models. In Figures 4a and 4b we take a look at one of the problem areas of the $M(3000)F_2$ -based h_mF_2 model. As noted earlier, the current IRI model does not reproduce the evening peak in h_mF_2 that is observed at the magnetic equator. Figure 4 shows that both new

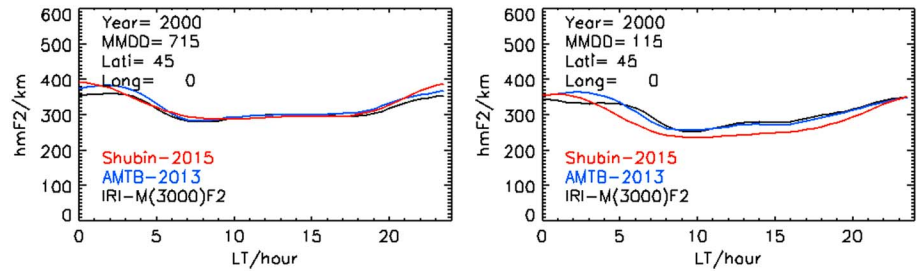


Figure 3. Comparison of the diurnal variation of the three IRI options for h_mF_2 at middle latitudes (geographic latitude/longitude = 45°/0°) for a (left) summer (15 July) and (right) winter (15 January) example for a year of high solar activity (2000).

models predict evening peaks and thus are a clear improvement over the older model. We note, however, that the two models predict the peak occurrence at different local times most clearly visible in the winter case in Figure 4b. Comparisons with measurements from techniques other than digisonde and RO are required to find out which one of these model predictions is closer to the real ionosphere. Figures 5a and 5b highlight differences in the solar cycle variation predicted by these three h_mF_2 models for a midlatitude location. The differences among these three models are largest in the solar minima and maxima reaching values of up to 40–50 km. At the solar minimum, the AMTB model is consistently higher than the other two models by about 30 km. At solar maximum, the SMDF2 model produces the largest values during nighttime and the smallest values during daytime. In particular, these last figures hint at the significant discrepancies that still exist between the h_mF_2 values measured from the ground with digisondes and those measured from a satellite with the RO technique. By offering both options, IRI lets users explore the effect that these uncertainties may have on their specific application. In the case of the ionosonde the assumption of a monotonously increasing bottomside profile can lead to errors of 10–20 km if a valley is present in the E region. RO errors can be even larger especially in the low-latitude region where the assumption of spherical symmetry breaks down. Because of the lower error estimates for ionosonde measurements IRI recommends the *Altadill et al.* [2013] model as its first choice.

3. Improvement of the on Composition Model in the Topside Ionosphere

The topside ion composition model in IRI provides the percentage of O^+ , H^+ , He^+ , and N^+ ions from the F_2 peak up to 2000 km. Two options are given, with the older *Danilov and Yaichnikov* [1985] model based on a compilation of Russian high-altitude rocket measurements and the newer model of *Třisková et al.* [2003] (TTS-03; the recommended default) based on in situ satellite measurements from IK-24, AE-C, and AE-E. The relatively small database used in the development of these model options limits their accuracy and reliability in areas not well covered by the database. Progress toward a better representation of ion composition in IRI has been slow because of calibration and contamination issues with some of the earlier satellite measurements and because of remaining discrepancies between ground and space-based observations [see *Bilitza et al.*, 2014, Figure 6]. The main problem of global modeling of ion composition is

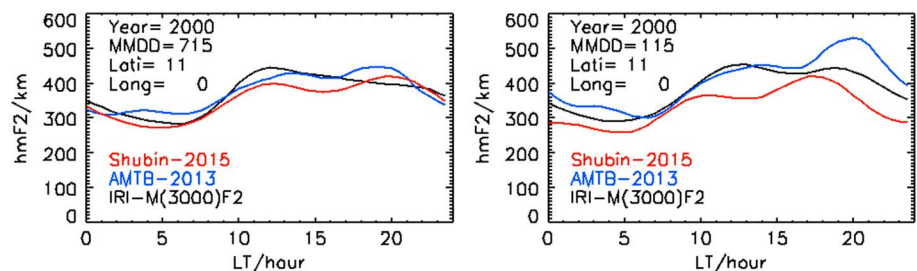


Figure 4. Comparison of the diurnal variation of the three IRI options for h_mF_2 at the magnetic equator (geographic latitude/longitude = 11°/0°) for a (left) summer (15 July) and (right) winter (15 January) example for a year of high solar activity (2000).

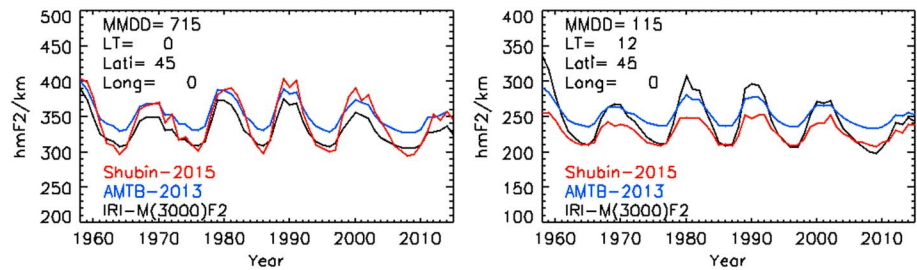


Figure 5. Comparison of the solar cycle variation of the three IRI options for h_mF_2 at middle latitudes (geographic latitude = $45^\circ/0^\circ$) for a (left) summer midnight (15 July, LT = 0:00) and (right) winter noon (15 January, LT = 12:00) example.

the relatively small database in comparison with other parameters like the electron density. The modeling has to rely on few mass spectrometer or retarding potential analyzer satellite experiments. Unfortunately, ion composition measurements by incoherent scatter radars or by rocket experiments are quite rare and their temporal and geographical coverage is insufficient for development of a global model. However, with the launch of the Communications/Navigation Outage Forecasting System (C/NOFS) satellite [*de La Beaujardière and the C/NOFS Definition Team, 2004*] in April 2008 a valuable new data source became available for modeling the ionospheric ion composition in the low-latitude region covered by this low-inclination satellite. The Coupled Ion Neutral Dynamics Instrument (CINDI) measured the ion composition in the latitude range 400–800 km from April 2008 to November 2015 when the satellite ceased operations. When comparing these new data with IRI predictions, *Heelis et al. [2009]* and *Coley et al. [2010]* found that IRI overestimated the percentage of O^+ ions in the topside ionosphere and underestimate the percentage of H^+ ions. The discrepancies were most pronounced during the solar minimum years 2008–2009. *Klenzing et al. [2011]* confirmed these results and further investigated the impact these misrepresentations have on the upper transition height h_t ; h_t is the height where the percentage of O^+ is equal to the percentage of light ions (50%), below h_t O^+ is the dominant ion, and above h_t H^+ and He^+ become the dominant ions. Efforts are underway to include this important transition parameter as one of the anchor points for the IRI ion composition model because of its added significance as marker for the transition from the ionosphere to the plasmasphere [*Bilitza, 1991*]. The 2008–2009 solar minimum was highly unusual in that it lasted longer than previous solar minima and reached a very low level of solar activity. IRI was built based on the existing data record, and since the 2008–2009 minimum conditions were so different from prior solar minima, it is not surprising, therefore, that the IRI model performed poorly.

For IRI-2016 a number of improvements of the TTS-03 model were implemented partly as a result of more old and newer data becoming available and partly in response to user-found errors and misrepresentations. *Truhlik et al. [2015]* were able to correct the model at low solar activities with the help of data from the C/NOFS-CINDI experiment. Improvements were also achieved at high solar activity with a more effective exploitation of the IK-24, AE-C, and AE-D database. Based on their analysis, the limits of allowable $F_{10.7}$ solar index values were extended from 85–200 in IRI-2012 to 65–260 in IRI-2016. The *Truhlik et al. [2015]* (TBT-15) model uses a similar formalism as TTS-03 for the representation of global variations, but instead of the linear $F_{10.7}$ dependence, it uses a logarithmic approach and instead of the percentages TBT-15 first models the absolute densities and then normalizes to 100%. The new model is also based on more data for solar minimum (two times more than in TTS-03) and for solar minimum uses 4 anchor points versus 3 in TTS-03. The impact of these improvements is documented in Figure 6. Shown here is the ratio between IRI predictions and the CINDI measurements of O^+ and H^+ ions versus solar activity averaged over the years 2008–2012. The dashed curves are using IRI-2012, and the solid curves are based on the new IRI-2016 ion composition model. For middle and high solar activities, the ratios are close to one underlining the good performance of the IRI model. With decreasing solar activity, the ratios for IRI-2012 deviate significantly from 1 reaching a ratio of 2 for the O^+ ions and of 0.6 for H^+ ions at the lowest level of solar activity. With IRI-2016 the ratios are now close to 1 over the whole solar activity range. Figure 7 highlights the success of the new model in lowering the transition height h_t from close to 1000 km down to almost 600 km which is closer to the h_t value reported with the CINDI measurements [*Klenzing et al., 2011*].

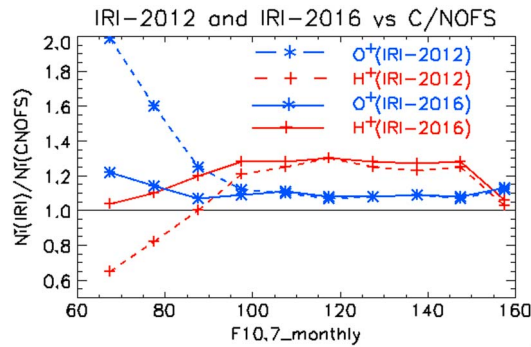


Figure 6. Ratio between IRI predictions and C/NOFS-CINDI measurements of O^+ (blue) and H^+ (red) densities versus the $F_{10.7}$ monthly solar index for IRI-2012 and the new IRI-2016. Note the large improvement at low solar activities.

Belgium, was the first solar index to be widely used in ionospheric modeling. Statistical studies showed highest correlation between R and ionosonde-measured f_oF_2 (the F_2 peak plasmas frequency) when averaged with a 12 month sliding window (denoted R_{12}). R_{12} is the solar activity index recommended by the International Telecommunication Union to describe the solar activity variation of its widely used *CCIR* [1967] model for f_oF_2 and the propagation factor $M(3000)F_2$. A recent review of the way R is determined from observations of spots on the Sun resulted in a recalibration of the R computation [Clette et al., 2014]. The new sunspot number is now internationally accepted and distributed by SIDC. It exceeds the old index by about a factor of 1.4. This revision of the sunspot index causes a problem for IRI and other models that were developed using the old R index. Using the new R with these models would result in a misrepresentation of the modeled parameters. To avoid this misrepresentation, IRI will use the new index with a scaling factor of 0.7. For the 12 month running mean 0.7 is a very good estimate for the ratio of these two indices [Gulyaeva, 2014].

4. Solar and Ionospheric Indices Used in IRI

The IRI model is driven by several solar and ionospheric indices: the sunspot number R , the solar radio flux at 10.7 cm wavelength $F_{10.7}$, and the ionosonde-based ionospheric global (I_G) index. An IRI user can rely on either the indices files that are part of the IRI distribution and that are updated twice a year or the user can enter his/her own values for these indices. We will briefly discuss these indices, recent changes in their production, and their role in the IRI model.

The sunspot number R that is provided by the Solar Influences Data analysis Center (SIDC, <http://sidc.oma.be>) in Brussels,

In IRI the R_{12} index is used for the F_2 peak height h_mF_2 , for the F_1 region plasma frequency f_oF_1 , for the bottomside thickness parameter B_o , and for the electron density at the D region inflection point.

The global daily value of the $F_{10.7}$ index is measured at local noon at the Penticon Radio Observatory in Canada since 1947. $F_{10.7}$ has been slowly replacing R in ionospheric modeling because it correlates better with the extreme ultraviolet (EUV) irradiance of the Sun that is responsible for the ionization of ions in the ionosphere. It has the added advantage that it can be measured directly at the ground and does not require an analysis scheme like the sunspot number. It is a very robust long-term measurement of solar activity with few gaps or calibration issues. Modelers have used different averages of the $F_{10.7}$ index from the daily index $F_{10.7}$ to the 81 day (three solar rotation) average $F_{10.7_{81}}$ to a 12 month running mean $F_{10.7_{12}}$. IRI makes use of all three indices. $F_{10.7}$ for the

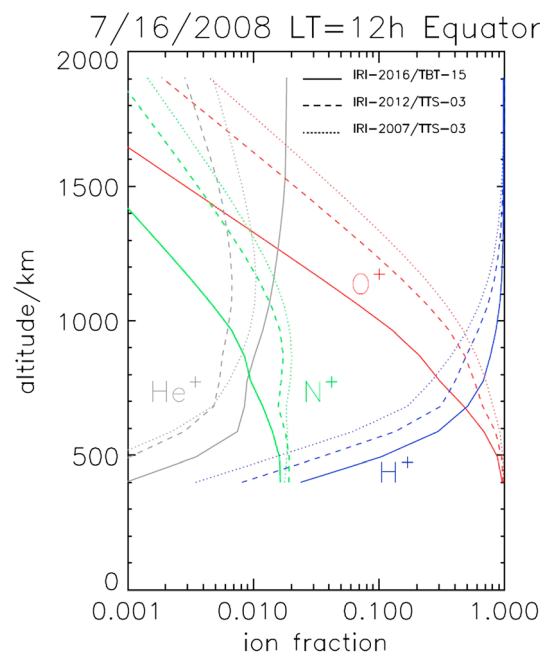


Figure 7. Topside ion composition with the IRI-2007 (dotted curves), IRI-2012 (dashed curves), and the new IRI-2016 models (solid curves). Note the steady decrease in upper transition height h_t from close to 1000 km in IRI-2007 to close to 700 km in IRI-2016.

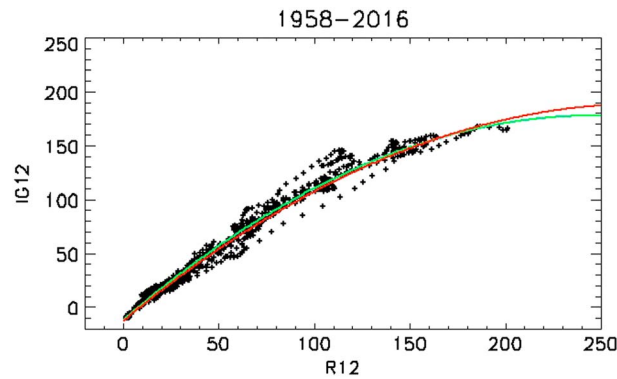


Figure 8. Correlation between the indices IG_{12} and R_{12} (+) over the time period from 1958 to 2016 and curves fitted: $IG_{12} = 12.349 + 1.468 \times R_{12} - 0.00268 \times (R_{12})^2$ (red; used in IRI), $IG_{12} = -11.563 + 1.533 \times R_{12} - 0.0031 \times (R_{12})^2$ (green; recommended by Gulyaeva [2014]).

previous day is needed as input for the NRL-MSISE00 model [Picone *et al.*, 2002] of the neutral temperatures and densities that are required as lower limits for the plasma temperatures and as input for the ion composition model [Richards *et al.*, 2010]. For the electron temperature the best results have been obtained with the composite index $PF_{10.7} = (F_{10.7} + F_{10.7_{81}}) / 2$ and this index is used in IRI for the electron temperature model. $PF_{10.7}$ is also used for the IRI topside ion composition by the TTS-03 model [Třisková *et al.*, 2003], while the older DY-85 option [Danilov and Yaichnikov, 1985] describes solar activity variations with the $F_{10.7_{12}}$ index.

The IG index was introduced by Liu *et al.* [1983]. It is obtained by adjusting the CCIR [1967] model for f_oF_2 to the noontime measurements of several reference ionosonde stations. This is achieved by changing the R_{12} index that describes the solar activity variations in the CCIR model. The final step is taking the average over all stations to generate the global IG index. It is produced and distributed by the UK Solar System Data Centre in Slough, England. The original index was produced based on 11 reference stations; however, not all of these stations have remained in operation or continued to be able to share their data. Currently the index is determined with four reference stations: two from the Southern Hemisphere (Port Stanley/UK and Canberra/Canada) and two from the Northern Hemisphere (Kokubunji/Japan and Chilton/UK). This has limited the reliability of this index in representing the global ionospheric conditions; nevertheless, it is still superior to the R and $F_{10.7}$ indices in describing the solar cycle changes in the F region ionosphere. In IRI the 12 month running mean IG_{12} is used with the CCIR [1967] f_oF_2 model and therefore has a strong impact on the whole electron density profile since it is normalized to the F_2 peak and since the ionosphere reaches its highest densities at the F_2 peak. As for the other indices, an IRI user has the option to use the internal indices file or to enter his/her own index value for IG_{12} . The long-term correlation function between IG_{12} and R_{12} (Figure 8) is used to automatically adjust IG_{12} if only R_{12} is entered and vice versa.

5. Real-Time IRI

Good progress has been made in the development of an IRI Real-Time model. The goal is to progress from the climatology provided by the standard IRI model to a description of real-time weather conditions based on the ingestion of real-time measurements into the IRI model. A number of studies have used ionosonde and/or GPS data to update the IRI model by adjusting the ionospheric and/or solar indices used in IRI with real-time ionosonde or TEC data [Bilitza *et al.*, 1997; Komjathy *et al.*, 1998; Hernandez-Pajares *et al.*, 2002; Pezzopane *et al.*, 2011; Ssessanga *et al.*, 2015]. Another group of studies have used the IRI as background ionosphere applying a Kalman filter or variational method to assimilate real-time data into IRI [Fridman *et al.*, 2006; Schmidt *et al.*, 2008; Angling *et al.*, 2009; Yue *et al.*, 2012; Galkin *et al.*, 2012]. These activities were discussed during several dedicated IRI Real-Time Workshop (see irimodel.org for more details) and have led to considerable improvements of these real-time algorithms.

The most advanced IRI Real-Time model is the IRI Real-Time Assimilative Modelling (IRTAM) system developed by Galkin *et al.* [2012] that assimilates digisonde data from the Global Ionospheric Radio Observatory (GIRO) network into the IRI model. The IRTAM approach is based on the CCIR [1967] models for the F_2 peak plasma frequency f_oF_2 and the propagation factor $M(3000)F_2$ that are being used in IRI. IRTAM uses the CCIR set of functions to describe the global and spatial variation of the difference between the digisonde measurement and the IRI prediction of f_oF_2 . The method consists of three steps: (1) expand the 24 h history of Δf_oF_2 at each station in sixth-order harmonics (13 coefficients ΔC_i); (2) interpolate each ΔC_i into (36×36) spatial grid using a multicell iterative optimization for interpolation smoothness via a neural network

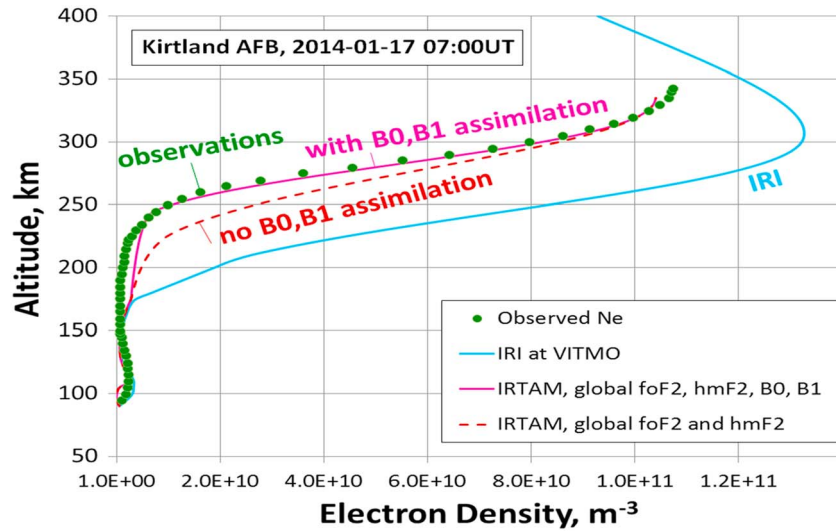


Figure 9. The measured and IRI-predicted electron density profile at Kirkland AFB on 17 January 2014 at 07:00 UT. Besides the densities measured by the digisonde (dots) the figure shows the standard IRI (blue solid curve), IRI with IRTAM f_oF_2 and h_mF_2 (red dashed curve) and IRI with IRTAM f_oF_2 , h_mF_2 , and B_0 and B_1 (red solid curve).

computation with fading synoptic weights; (3) fit each of the grids with the CCIR [1967] set of geographic functions (76 coefficients) to obtain $13 \times 76 = 988$ corrections ΔC_{ik} . Adding the correction terms to the original CCIR coefficients produces the IRI Real-Time model of f_oF_2 . The same procedure is used for the height of the F_2 peak, h_mF_2 . There is, however, an important difference, the parameter mapped in CCIR is $M(3000)F_2$ and not h_mF_2 . IRI determines h_mF_2 with the help of the *Bilitza et al.* [1979] model that describes

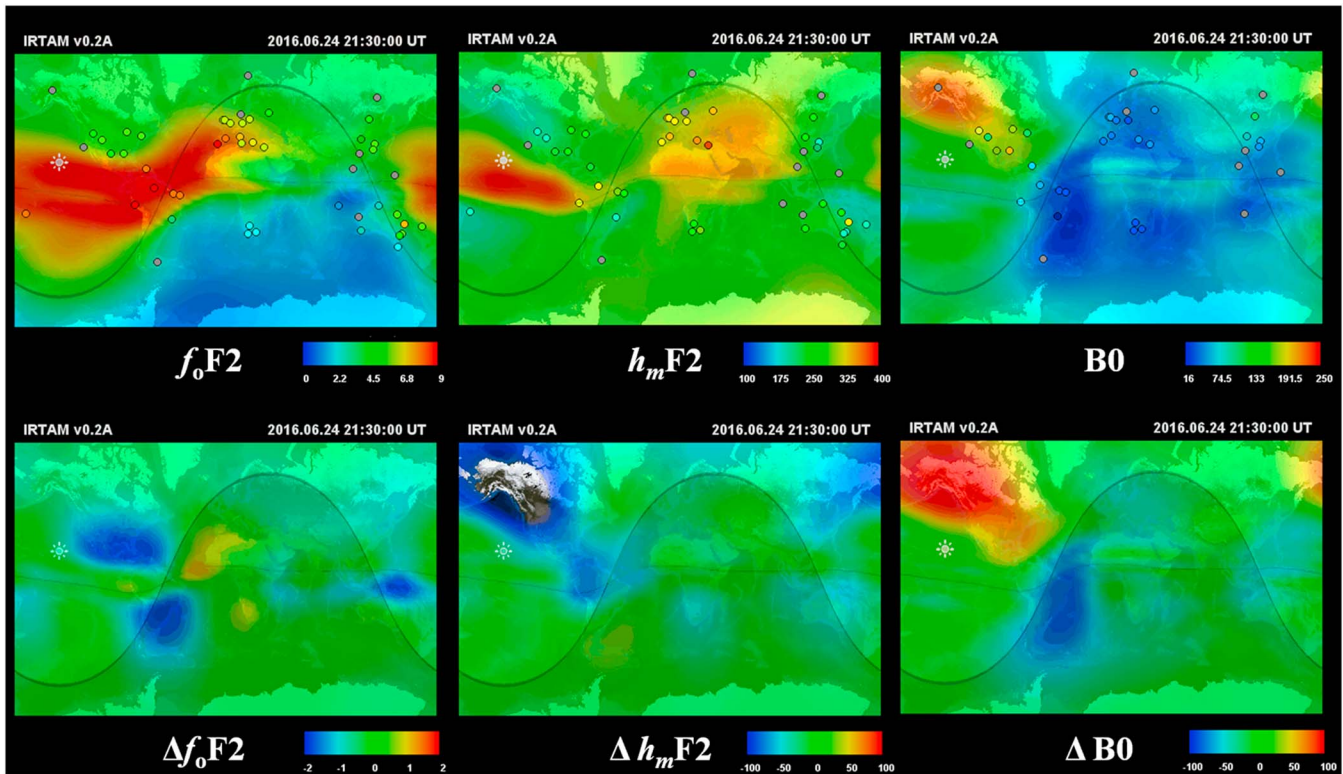


Figure 10. IRTAM global predictions for (top row) f_oF_2 , h_mF_2 , and B_0 for 24 June 2016 at 21:30:00 UT. The circles in Figure 10 (top row) mark the locations of digisonde stations, and their color gives the magnitude of the measured parameters. (bottom row) The global differences maps between measured and predicted parameters. The solid curve in all panels marks the terminator.

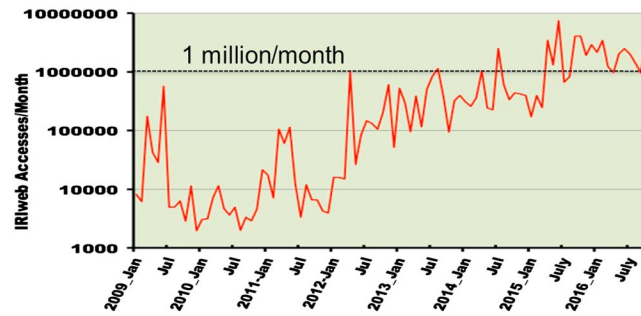


Figure 11. Monthly accesses to the online IRIweb service. Only accesses to the SPDF site are counted. Accesses to the CCMC site are not included. Note the logarithmic scale indicating an exponential increase in accesses over the last 6 years.

the correlation between $M(3000)F_2$ and h_mF_2 . Here the work of *Brunini et al.* [2013] was of great help because they had already used the CCIR formalism to represent the IRI- h_mF_2 directly. Starting from this CCIR-type representation of h_mF_2 , the process is then the same as for f_oF_2 . The latest and newest addition to the IRI parameters that are being provided in real time is the bottom-side thickness B_0 and the bottomside shape parameter B_1 . The approach is the same as for h_mF_2 ; the first step,

however, is the representation of the IRI- B_0 and IRI- B_1 in CCIR-type models that were then updated with real-time digisonde measurements in the same way as f_oF_2 . Figure 9 shows that assimilation of B_0 and B_1 is critical to the accuracy of the IRTAM electron density profiles. Using only f_oF_2 and h_mF_2 assimilation without also assimilating the measured B_0 , B_1 values can produce a wrong bottomside electron density profile.

In addition, the latest version of IRTAM introduces a new trend term (fourteenth coefficient) this was necessary to relax the 24 h periodicity requirement of the CCIR [1967] basis model. An example of IRTAM predictions for f_oF_2 , h_mF_2 and B_0 is shown in Figure 10 including also the location of the digisondes used and the differences between measurements and predictions at each station (color in station circle). A first preliminary evaluation including 15 million points found an average improvement factor of ~ 2 when using IRI with IRTAM versus the standard IRI without IRTAM.

6. Summary

This article introduces and discusses the 2016 version of the International Reference Ionosphere model. The most important improvements are as follows:

1. There are two new model options for the F_2 peak height h_mF_2 , one based on digisonde data [Altadill et al., 2013] and one based on radio occultation data [Shubin, 2015]. Most significantly, these new options are now modeling h_mF_2 directly and no longer through its relationship to the propagation factor $M(3000)F_2$. The digisonde-based model is the recommended choice in IRI-2016. Our comparisons of these models highlight areas and time periods where significant differences exist that warrant further study and a call for more direct measurements of h_mF_2 .
2. There is a more accurate and reliable description of the topside ion composition at low solar activities based on C/NOFS-CINDI data.
3. IRI-2016 accounts for the newly revised sunspot number index in the IRI model parts that depend on this parameter.

Significant advances have been made in the development of a Real-Time IRI model. The IRI Real-Time Assimilative Modeling (IRTAM) now assimilates real-time measurements of f_oF_2 , h_mF_2 , B_0 , and B_1 from 40+ digisonde stations into IRI and first test have shown an improvement of a factor of 2 compared to the standard IRI and even larger during disturbed time periods. The next steps will be the inclusion of real-time measurements of h_mF_1 , f_oF_1 , C_1 , h_mE , and f_oE in the IRTAM process.

Table 1. Percentage of Papers That Acknowledge the Use of IRI in the Journal of Geophysical Research (JGR), the Geophysical Research Letters (GRL), the Space Weather (SW) Journal, and Radio Science (RS)

Year	JGR	GRL	SW	RS
2009	5.0%	3.6%	0.0%	10.5%
2010	5.6%	4.7%	5.6%	11.8%
2011	7.1%	1.6%	8.1%	14.2%
2012	7.6%	2.7%	4.8%	13.8%
2013	5.1%	1.7%	2.3%	8.2%
2014	6.6%	0.5%	5.7%	10.7%
2015	8.3%	2.3%	1.6%	9.6%
2016	6.8%	0.8%	2.2%	13.2%

More information about the IRI activities including publications and workshops can be found on the homepage irmodel.org, which also provides access to the IRI FORTRAN code and the IRIweb service. The continued wide usage of the IRI model is documented in Figure 11 and Table 1. Figure 11 plots the monthly accesses to IRIweb since January 2009. IRIweb is an online service for the computation and plotting of IRI parameter profiles for user-provided location and time. The services can be also accessed via web services. Figure 11 illustrates the steady increase in IRI usage reaching now 5 million accesses per month. Actual usage of this service is even higher because we are not counting the accesses to the parallel site maintained by the Community Coordinated Modeling Center (CCMC).

Table 1 reports the acknowledged use of the IRI model in the scientific journals *Journal of Geophysics-Space Physics* (JGR-SP), *Geophysical Research Letters*, *Radio Science* (RS), and *Space Weather*. The numbers in Table 1 are the percentage of papers of a specific year that made use of the IRI model. In 2015 a remarkable 8% of JGR-SP papers and 10% (!) of RS papers relied on IRI for their studies.

Acknowledgments

We like to acknowledge the IRI Working Group with all its members for their support of the IRI activities. We like to dedicate this paper to our coauthor Xueqin Huang who passed away on 15 October 2016. Xueqin was a member of the IRI Working Group and contributed key IRI improvements. We thank NASA's Space Physics Data Facility (SPDF) and Community Coordinated Modeling Center (CCMC) for the IRIweb online computation service. B.R., X.H., I.G., and D.B. were in part supported by USAF contracts FA9453-14-C-0305 and FA865016C9104. D.A. is in part supported by Universitat Ramon Llull project 2016-URL-Trac-001 funded by "Obra Social la Caixa" and by Spanish Ministry MINECO through project CTM2014-52182-C3-1-P. V.T. was supported, in part, by grant 15-07281J of the Grant Agency of the Czech Republic. V.S. was supported by the Russian Foundation for Basic Research through project 17-05-00427. The IRI model code in Fortran is available from the IRI homepage at irmodel.org.

References

- Abdu, M. A., I. S. Batista, C. G. M. Brum, J. W. MacDougall, A. M. Santos, J. R. de Souza, and J. H. A. Sobral (2010), Solar flux effects on the equatorial evening vertical drift and meridional winds over Brazil: A comparison between observational data and the IRI model and the HWM representations, *Adv. Space Res.*, *46*, 1078–1085, doi:10.1016/j.asr.2010.06.009.
- Adeniyi, J., D. Bilitza, S. Radicella, and A. Willoughby (2003), Equatorial F₂-peak parameters in the IRI model, *Adv. Space Res.*, *31*(3), 507–512, doi:10.1016/S0273-1177(03)00039-5.
- Altadill, D., S. Magdaleno, J. M. Torta, and E. Blanch (2013), Global empirical models of the density peak height and of the equivalent scale height for quiet conditions, *Adv. Space Res.*, *52*, 1756–1769, doi:10.1016/j.asr.2012.11.018.
- Angling, M. J., J. Shaw, A. K. Shukla, and P. S. Cannon (2009), Development of an HF selection tool based on the Electron Density Assimilative Model near-real-time ionosphere, *Radio Sci.*, *44*, RS0A13, doi:10.1029/2008RS004022.
- Araujo-Pradere, E. A., D. Buresova, D. J. Fuller-Rowell, and T. J. Fuller-Rowell (2013), Initial results of the evaluation of IRI hmF₂ performance for minima 22–23 and 23–24, *Adv. Space Res.*, *51*, 630–638, doi:10.1016/j.asr.2012.02.010.
- Bilitza, D. (1985), Comparison of measured and predicted F₂ peak altitudes, *Adv. Space Res.*, *5*(10), 29–32, doi:10.1016/0273-1177(85)90176-0.
- Bilitza, D. (1991), The use of transition heights for the representation of ion composition, *Adv. Space Res.*, *11*(10), 183–186, doi:10.1016/0273-1177(91)90341-G.
- Bilitza, D., and R. Eyfrig (1978), Model zur Darstellung der Höhe des F₂-Maximums mit Hilfe des M(3000)F₂ Wertes des CCIR (German), *Kleinheubacher Ber.*, *21*, 167–174.
- Bilitza, D., N. Sheik, and R. Eyfrig (1979), A global model for the height of the F₂-peak using M3000 values from the CCIR numerical map, *Telecommun. J.*, *46*, 549–553.
- Bilitza, D., S. Bhardwaj, and C. Koblinsky (1997), Improved IRI predictions for the GEOSAT time period, *Adv. Space Res.*, *20*(9), 1755–1760, doi:10.1016/S0273-1177(97)00585-1.
- Bilitza, D., D. Altadill, Y. Zhang, C. Mertens, V. Truhlik, P. Richards, L.-A. McKinnell, and B. Reinisch (2014), The International Reference Ionosphere 2012—A model of international collaboration, *J. Space Weather Space Clim.*, *4*, 1–12, doi:10.1051/swsc/2014004.
- Blanch, E., and D. Altadill (2012), Midlatitude F region peak height changes in response to interplanetary magnetic field conditions and modeling results, *J. Geophys. Res.*, *117*, A12311, doi:10.1029/2012JA018009.
- Brum, C. G. M., F. S. Rodrigues, P. T. dos Santos, A. C. Matta, N. Aponte, S. A. Gonzalez, and E. Robles (2011), A modeling study of f_oF_2 and h_mF_2 parameters measured by the Arecibo incoherent scatter radar and comparison with IRI model predictions for solar cycles 21, 22, and 23, *J. Geophys. Res.*, *116*, A03324, doi:10.1029/2010JA015727.
- Brunini, C., J. F. Conte, F. Azpilicueta, and D. Bilitza (2013), A different method to determine the height of the F₂ peak, *Adv. Space Res.*, *51*, 2322–2332, doi:10.1016/j.asr.2013.01.027.
- CCIR (1967), Consultative Committee on International Radio, Atlas of ionospheric characteristics Report 340, International telecommunication Union, Geneva, Switzerland.
- Clette, F., L. Svalgaard, J. M. Vaquero, and E. W. Cliver (2014), Revisiting the sunspot number—A 400-year perspective on the solar cycle, *Space Sci. Rev.*, *186*, 35–103, doi:10.1007/s11214-014-0074-2.
- Coley, W. R., R. A. Heelis, M. R. Hairston, G. D. Earle, M. D. Perdue, R. A. Power, L. L. Harmon, B. J. Holt, and C. R. Lippincott (2010), Ion temperature and density relationships measured by CINDI from the C/NOFS spacecraft during solar minimum, *J. Geophys. Res.*, *115*, A02313, doi:10.1029/2009JA014665.
- Danilov, A. D., and A. P. Yaichnikov (1985), A new model of the ion composition at 75 to 1000 km for IRI, *Adv. Space Res.*, *5*(7), 75–79, doi:10.1016/0273-1177(85)90360-6.
- de La Beaujardière, O., and the C/NOFS Definition Team (2004), C/NOFS: A mission to forecast scintillations, *J. Atmos. Sol.-Terr. Phys.*, *66*, 1573–1591, doi:10.1016/j.jastp.2004.07.030.
- Dudeney, J. R. (1983), The accuracy of simple methods A simple empirical method for determine the height of the maximum electron concentration of the F₂-layer from scaled ionospheric characteristics, *J. Atmos. Sol. Terr. Phys.*, *45*(8/9), 629–640, doi:10.1016/S0021-9169(83)80080-4.
- Dyson, P. L., T. P. Davies, M. L. Parkinson, A. J. Reeves, P. G. Richards, and C. E. Fairchild (1997), Thermospheric neutral winds at southern mid-latitudes: A comparison of optical and ionosonde h_mF_2 methods, *J. Geophys. Res.*, *102*(A12), 27,189–27,196, doi:10.1029/97JA02138.
- Ezquer, R. G., J. L. López, L. A. Scidá, M. A. Cabrera, B. Zolesi, C. Bianchi, M. Pezzopane, E. Zuccheretti, and M. Mosert (2014), Behavior of ionospheric magnitudes of F₂ region over Tucumán during a deep solar minimum and comparison with the IRI2012 model predictions, *J. Atmos. Sol. Terr. Phys.*, *107*, 89–98, doi:10.1016/j.jastp.2013.11.010.
- Fridman, S. V., L. J. Nickisch, M. Aiello, and M. Hausman (2006), Real-time reconstruction of the three-dimensional ionosphere using data from a network of GPS receivers, *Radio Sci.*, *41*, RS5512, doi:10.1029/2005RS003334.
- Galkin, I. A., B. W. Reinisch, X. Huang, and D. Bilitza (2012), Assimilation of GIRO data into a real-time IRI, *Radio Sci.*, *47*, RS0L07, doi:10.1029/2011RS004952.

- Gulyaeva, T. L. (2012), Empirical model of ionospheric storm effects on the F_2 layer peak height associated with changes of peak electron density, *J. Geophys. Res.*, *117*, A02302, doi:10.1029/2011JA017158.
- Gulyaeva, T. L. (2014), Modification of solar activity indices in the International Reference Ionosphere IRI and IRI-Plas models due to recent revision of sunspot number time series, *Sol. Terr. Phys.*, *2*(3), 59–66, doi:10.12737/20872.
- Gulyaeva, T. L., P. A. Bradley, I. Stanislawska, and G. Juchnikowski (2008), Towards a new reference model of hmF_2 for IRI, *Adv. Space Res.*, *42*, 666–672, doi:10.1016/j.asr.2008.02.021.
- Heelis, R. A., W. R. Coley, A. G. Burrell, M. R. Hairston, G. D. Earle, M. D. Perdue, R. A. Power, L. L. Harmon, B. J. Holt, and C. R. Lippincott (2009), Behavior of the O^+/H^+ transition height during the extreme solar minimum of 2008, *Geophys. Res. Lett.*, *36*, L00C03, doi:10.1029/2009GL038652.
- Hernandez-Pajares, M., J. Juan, J. Sanz, and D. Bilitza (2002), Combining GPS measurements and IRI model values for Space Weather specification, *Adv. Space Res.*, *29*(6), 949–958, doi:10.1016/S0273-1177(02)00051-0.
- Hoque, M. M., and N. Jakowski (2012), A new global model for the ionospheric F_2 peak height for radio wave propagation, *Ann. Geophys.*, *30*, 797–809, doi:10.5194/angeo-30-797-2012.
- Huang, X., and B. W. Reinisch (1996), Vertical electron density profiles from digisonde ionograms. The average representative profile, *Ann. Geophys.*, *39*(4), 751–756, doi:10.4401/ag-4010.
- Jones, W., and R. Gallet (1962), Representation of diurnal and geographic variations of ionospheric data by numerical methods, *J. Res. Natl. Bur. Stand.*, *66D*(4), 419–438.
- Klenzing, J., F. Simões, S. Ivanov, R. A. Heelis, D. Bilitza, R. Pfaff, and D. Rowland (2011), Topside equatorial ionospheric density and composition during and after extreme solar minimum, *J. Geophys. Res.*, *116*, A12330, doi:10.1029/2011JA017213.
- Komjathy, A., R. Langley, and D. Bilitza (1998), Ingesting GPS-derived TEC data into the International Reference Ionosphere for single frequency radar altimeter ionospheric delay corrections, *Adv. Space Res.*, *22*(6), 793–802, doi:10.1016/S0273-1177(98)00100-8.
- Lee, C.-C., and B. W. Reinisch (2006), Quiet-condition hmF_2 , NmF_2 , and B_0 variations at Jicamarca and comparison with IRI-2001 during solar maximum, *J. Atmos. Sol. Terr. Phys.*, *68*, 2138–2146, doi:10.1016/j.jastp.2006.07.007.
- Liu, R., P. Smith, and J. King (1983), A new solar index which leads to improved foF2 predictions using the CCIR Atlas, *Telecommun. J.*, *50*, 408–414.
- Magdalenó, S., D. Altadill, M. Herraiz, E. Blanch, and B. de la Morena (2011), Ionospheric peak height behavior for low middle and high latitudes: A potential empirical model for quiet conditions—Comparison with the IRI-2007 model, *J. Atmos. Sol. Terr. Phys.*, *73*, 1810–1817, doi:10.1016/j.jastp.2011.04.019.
- Miller, K. L., D. G. Torr, and P. G. Richards (1986), Meridional winds in the thermosphere derived from measurement of F_2 layer height, *J. Geophys. Res.*, *91*(A4), 4531–4535, doi:10.1029/JA091iA04p04531.
- Miller, K. L., M. Lemon, and P. G. Richards (1997), A meridional wind climatology from a fast model for the derivation of meridional winds from the height of the ionospheric F_2 region, *J. Atmos. Sol. Terr. Phys.*, *59*(14), 1805–1822, doi:10.1016/S1364-6826(97)00025-4.
- Pezzopane, M., M. Pietrella, A. Pignatelli, B. Zolesi, and L. R. Cander (2011), Assimilation of autoscaled data and regional and local ionospheric models as input sources for real-time 3-D International Reference Ionosphere modeling, *Radio Sci.*, *46*, RS5009, doi:10.1029/2011RS004697.
- Picone, J. M., A. E. Hedin, D. P. Drob, and A. C. Aikin (2002), NRLMSISE-00 empirical model of the atmosphere: Statistical comparisons and scientific issues, *J. Geophys. Res.*, *107*(A12), 1468, doi:10.1029/2002JA009430.
- Reinisch, B. W., and I. A. Galkin (2011), Global Ionospheric Radio Observatory (GIRO), *Earth Planets Space*, *63*(4), 377–381, doi:10.5047/eps.2011.03.001.
- Richards, P. G. (1991), An improved algorithm for determining neutral winds from the height of the F_2 peak electron density, *J. Geophys. Res.*, *96*, 17,839–17,846, doi:10.1029/91JA01467.
- Richards, P. G., D. Bilitza, and D. Voglozin (2010), Ion density calculator (IDC): A new efficient model of ionospheric ion densities, *Radio Sci.*, *45*, RS5007, doi:10.1029/2009RS004332.
- Schmidt, M., D. Bilitza, C. K. Shum, and C. Zeilhofer (2008), Regional 4-D modeling of the ionospheric electron density, *Adv. Space Res.*, *42*(4), 782–790, doi:10.1016/j.asr.2007.02.050.
- Shimazaki, T. (1955), World-wide daily variations in the height of the electron density of the ionospheric F_2 -layer, *J. Radio Res. Lab.*, *2*, 85–97.
- Shubin, V. N. (2015), Global median model of the F_2 -layer peak height based on ionospheric radio-occultation and ground-based digisonde observations, *Adv. Space Res.*, *56*, 916–928, doi:10.1016/j.asr.2015.05.029.
- Shubin, V. N., A. T. Karpachev, and K. G. Tsybulya (2013), Global model of the F_2 layer peak height for low solar activity based on GPS radio-occultation data, *J. Atmos. Sol. Terr. Phys.*, *104*, 106–115, doi:10.1016/j.jastp.2013.08.024.
- Ssessanga, N., Y. H. Kim, E. Kim, and J. Kim (2015), Regional optimization of the IRI-2012 output (TEC, foF2) by using derived GPS-TEC, *J. Korean Phys. Soc.*, *66*(10), 1599–1610, doi:10.3938/jkps.66.1599.
- Trísková, L., V. Truhlík, and L. Šmilauer (2003), An empirical model of ion composition in the outer ionosphere, *Adv. Space Res.*, *31*(3), 653–663, doi:10.1016/S0273-1177(03)00040-1.
- Truhlík, V., D. Bilitza, and L. Trísková (2015), Towards better description of solar activity variations in IRI ion composition model, *Adv. Space Res.*, *55*(8), 2099–2105, doi:10.1016/j.asr.2014.07.033.
- Yue, X., et al. (2012), Global 3-D ionospheric electron density reanalysis based on multi-source data assimilation, *J. Geophys. Res.*, *117*, A09325, doi:10.1029/2012JA017968.
- Zhang, M.-L., C. Liu, W. Wan, L. Liu, and B. Ning (2009), A global model of the ionospheric F_2 peak height based on EOF analysis, *Ann. Geophys.*, *27*, 3203–3212, doi:10.5194/angeo-27-3203-2009.

Erratum

In the originally published version of this article, several instances of text were incorrectly typeset. The following have since been corrected and this version may be considered the authoritative version of record. In Table 1, in the year column “2014” was repeated 3 times. It now reads “2014, 2015, 2016”.